



Experimental Investigation of the Direct Shear Strength Parameters of Compacted Snow

Haifeng Huo ^{1, 2}, Hui Xu ¹, Jixiu Wu ^{3*}, Tao Li ¹, Jingjin Liu ⁴, Enzhao Xiao ⁵, Xueyuan Tang ⁵

- ¹College of Transportation Science and Engineering, Civil Aviation University of China, Tianjin 300300, China
- ²Airport Engineering Safety and Long-term Performance Research Base of the Ministry of Transport, Tianjin 300300, China ³Technology Innovation Center for Directional Drilling Engineering, Ministry of Natural Resources, Langfang 065000, China
 - ⁴Dept. of Civil Engineering, Tianjin Univ., Tianjin 300350, China
 - ⁵R & D Division of Polar Snow and Ice Runways, Polar Research Institute of China, Shanghai 201209, China
- 10 Correspondence to: Jixiu Wu (272139943@qq.com)

Abstract. Compacted snow is utilized as a building material in various construction and engineering applications across global high-latitude regions. For the safety assessment of snow and ice structures in cold regions, cohesion and internal friction angle are key shear strength parameters for compacted snow. This study investigates 69 test conditions, considering variations in initial density, sintering time, and sintering temperature. Using direct shear tests, the variation patterns of the shear strength of compacted (machine-made) snow under normal pressures below 100 kPa were analyzed. Results show that under high sintering degree conditions and low normal pressures, the shear stress—displacement curve tends to exhibit strain softening. As initial density increases from 450 to 650 kg·m⁻³, both cohesion and internal friction angle increase linearly. With sintering time increasing from 0 to 60 days, cohesion first rises and then falls, while the internal friction angle steadily decreases. As sintering temperature decreases from -5 to -25°C, cohesion decreases, whereas the internal friction angle increases slightly. A Genetic Algorithm-Back Propagation (*GA-BP*) neural network was employed to develop a predictive model for shear strength parameters, providing benchmark values for cohesion and internal friction angle under various conditions. These benchmarks can be adaptively adjusted when additional influencing factors require consideration. This study provides essential strength parameters for the design and construction of compacted snow structures and offers a framework for accounting for the influence of other factors on these parameters.

25 1 Introduction

15

Compacted snow is utilized as a building material for infrastructure in high-latitude regions, including runways and pavement structures, etc. (Ager, 1960; Putkisto, 1959; Sun et al., 2021). In assessing the safety of compacted snow layers, shear strength is a critical mechanical indicator (Abele, 1967; McClung, 1979), which is significantly influenced by environmental and construction factors. Deeper snow layers, having undergone prolonged natural compaction and sintering, possess greater mechanical strength, which consequently increases the difficulty of construction handling. Therefore, compaction and sintering processes are primarily employed on surface snow in engineering practice (Sun et al., 2021).



50

65



Compaction increases snow density, thereby enhancing its frictional strength (Li et al., 2024). Large sintering times promote the formation of bonds among ice particles (Colbeck, 1983; Wei et al., 2024; Demmenie et al., 2025), which improves intergranular bonding strength (Hong et al., 2022; Wei et al., 2024). Additionally, lower temperatures slow down the sintering process (Abele, 1990); consequently, the temperature of the snow layer is often raised to accelerate sintering and rapidly attain the target engineering strength (White, 2023). Furthermore, initial density, sintering time, and sintering temperature are known to significantly affect the strength development of compacted snow (Sun et al., 2021).

Previous studies have primarily examined the variation patterns of shear strength under different influencing factors through laboratory and field experiments. Butkovich (1958) and Ballard et al. (1965) investigated the relationship between shear strength and density, finding that shear strength increases exponentially with density. Snow with a higher degree of sintering exhibits greater shear strength (Ballard, 1965; Podolskiy, 2014), and the rate of this process is largely controlled by temperature—higher sintering temperatures accelerate sintering and lead to a rapid increase in strength over a short period (Abele, 1990). Conversely, higher shearing temperatures reduce the shear strength of snow (Ballard et al., 1965; Schweizer, 1998; Perla and Beck, 1982). Shear strength is also influenced by snow particle morphology (De Biagi et al., 2019), with different snow types showing varying strengths. For example, depth hoar (Perla and Beck, 1982; Keeler, 1968; Fukuzawa, 1993) and graupel (Abe, 2004) possess lower shear strength compared to fresh snow, while wet snow exhibits lower shear strength than dry snow (Yamano, 2002). Shear rate exerts a pivotal influence on snow strength and failure modes. With increasing shear rates, shear strength initially increases before declining, while higher rates trigger a transition in failure behavior from ductile to brittle (McClung, 1977; De Montmollin, 1982; Puzrin et al.,2019). De Montmollin (1982) classified failure modes under varying shear rates and found that both shear strength and residual stress after brittle failure decrease with increasing shear rate in the medium to high range.

Numerous studies have focused on the development of shear strength testing devices and methods (Barbero et al.,2016; Nakamura et al.,2010). The shear frame, a device specifically designed to measure the shear strength of snow under static loads, is widely used due to its convenient operation (Abe, 2004; Abe, 2006; Fohn, 1997; Jamieson, 2001; Perla and Beck, 1983). However, the shear frame exhibits significant variability in sample measurement, making it difficult to achieve high precision. To overcome this limitation, Barbero (2016) developed a device for in-situ direct shear testing capable of obtaining undisturbed snow samples. To replicate in-situ results under laboratory conditions, Reiweger (2010) designed an instrument that allows for shearing of both homogeneous and layered snow, enabling shearing in a tilted configuration to simulate actual snow slope conditions. Additionally, to quantitatively examine the effects of sintering, Podolskiy (2013) developed a shear apparatus that can be used to evaluate the contribution of sintering to snow strength.

While previous research has primarily examined the variation patterns of shear strength in compacted snow, few studies have conducted quantitative analyses of key strength parameters—cohesion and internal friction angle—which are essential for engineering evaluations. Most existing studies focus on low-density snow, whereas compacted snow used in engineering applications typically has high density ($\geq 500 \text{ kg} \cdot \text{m}^{-3}$). In this study, high-density snow samples were prepared using machine-made snow. A total of 69 test conditions were designed, considering variations in initial density, sintering time, and





sintering temperature, and direct shear tests were conducted on compacted snow. The evolution of shear stress—displacement curves was analyzed, and the variation patterns of cohesion and internal friction angle were identified. A Genetic Algorithm-Back Propagation (*GA-BP*) neural network was used to develop a predictive model for strength parameters under multivariable coupling conditions, and benchmark values for cohesion and internal friction angle were proposed. The findings of this study provide both theoretical insight and experimental data to support the design and construction of ice and snow engineering projects.

2 Test Scheme

70

2.1 Sample Preparation

The test samples were artificially produced using machine-made snow through a process of atomization, cooling, and crystallization, closely mimicking the natural formation of snow. During snow sample-making progress, a high-pressure pump inside the snowmaking machine pressurized water to 6 MPa, which was then atomized into fine mist via a specially designed nozzle. This mist was propelled by a high-speed fan, allowing it to travel a certain distance. Under subzero temperatures, the mist rapidly cooled upon contact with the air, forming ice nuclei that subsequently absorbed ambient water vapor to generate snow particles.

Environmental conditions during snow sample-making were maintained at -5 °C, 30 % relative humidity, wind speed ranges from 6 to 7 m·s⁻¹, with snow sample-making machine elevation angle of 45°, and the distance for the machine to spray snow is 10 m. The snow samples had a plate-like morphology with particle sizes ranging from approximately 0.8 to 1 mm. After collection, the snow samples were transferred to cold storage at -10 °C and 60 % humidity for rapid sample preparation. The preparation process included the following steps:

- (1) Compaction: a ring formwork with an inner diameter of 61.8 mm and a height of 20 mm was used. Snow of a predetermined mass was evenly filled into the ring formwork and compacted to achieve the desired initial density. Fig. 1 shows the resulting compacted sample.
 - (2) Sintering: the compacted sample, still within the ring formwork, was sealed externally with a membrane. Uniform snowflakes were spread around the sample to replicate a natural sintering environment. The sample was then placed in a test chamber set to a specific temperature and left to sinter for the designated duration.







Figure 1: Compacted specimen.

2.2 Test Equipment

100

Direct shear equipment used in the test is shown in Fig. 2. The shear box holds cylindrical snow samples with a diameter of 61.8 mm and a height of 20 mm. Normal stress is applied using a system of weights and a lever, while horizontal shear force is delivered by a motor operating at a constant rate. The device is capable of shearing four samples simultaneously, with a controllable shear rate ranging from 0 to 2.4 mm·min⁻¹.

The equipment shearing process is shown in Fig. 3. The normal stress system is connected to a lever and weights, while the drive system is linked to an electric motor. The shear box comprises upper and lower sections, with the specimen placed inside. During shearing, the upper box remains stationary, and the lower box equipped with ball bearings at its base, undergoes horizontal displacement via the drive system. A dynamometer is mounted on the upper box. No initial shear plane is predefined in the specimen; shear failure develops naturally through relative movement between the upper and lower boxes.



Figure 2: Direct shear equipment.





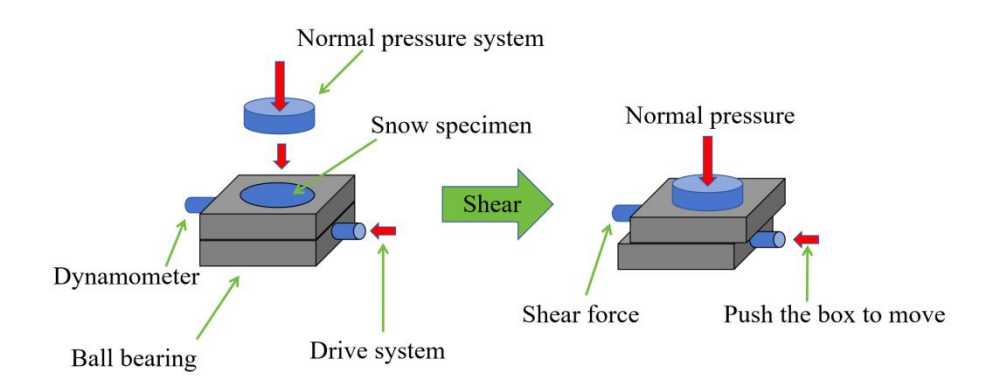


Figure 3: Equipment shearing process.

2.3 Test Procedure

Shearing rate directly influences the failure mode and strength characteristics of construction materials both in soil and snow-ice materials. Fig. 4 illustrates the variation in shear strength of snow with varying shear strain rate (redrawing from Puzrin et al., (2019)), generally showing an initial increase followed by a decreasing trend, while the strength parameters also change accordingly. From the perspective of engineering design, however, site investigation reports must provide quantitative characteristic values of strength parameters as a basis for structural design. Chinese Geotechnical Testing Standard (GB/T 50123) specifies a constant shearing rate of 0.8 mm·min⁻¹ for the quick direct shear test of soils. Therefore, the shear rate of snow was set at a constant value of 0.8 mm·min⁻¹ in this study. The shear strain rate is about 6.67×10⁻⁴ s⁻¹, which is in the gray area in Fig. 4. This study also follows the sample dimension, testing process, standard shear rate, and strength value methods used in soil mechanics. Analysis of the test data shows that, the shear stress-displacement curves of snow under this shearing rate exhibit both peak and non-peak types, which are all similar to soil test results. Nevertheless, both the failure modes and the strength variations exhibited clear and consistent patterns.





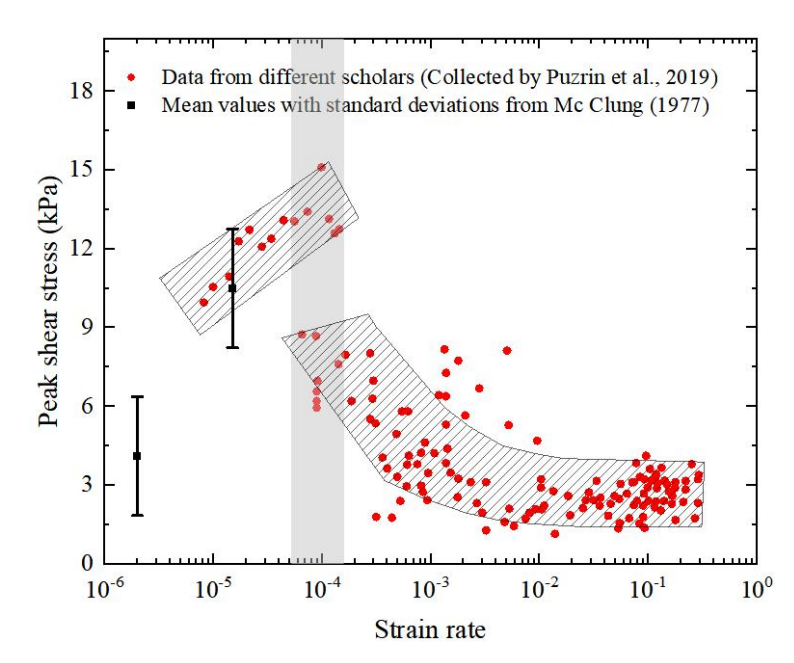


Figure 4: Variation of shear strength with shear strain rate (Redrawing from Puzrin et al., (2019))

Snow is a particular construction material, which testing apparatus and methods for obtaining mechanical parameters are often adapted from geotechnical engineering practices (Abele,1967,1990; White,2020). Therefore, this study strictly adhered to International Geotechnical Testing Standard (ISO 17892-10) and Chinese Geotechnical Testing Standard (GB/T 50123).

120 Direct shear test procedure is as follows:

125

130

specimen.

- (1) Demolding: the sintered sample was carefully and slowly removed from the ring formwork to avoid structural damage.
- (2) Shearing: the demolded sample was placed into the direct shear apparatus, and normal pressures of 25 kPa, 50 kPa, 75 kPa, and 100 kPa were applied. Shear loading was applied horizontally at a constant rate of 0.8 mm·min⁻¹, with the ambient temperature maintained at -10°C. To ensure thermal consistency, the shear apparatus was preconditioned in cold storage for 2 hours prior to testing so that the temperature of the shear box matched the test environment. Fig. 5 shows the sheared
- (3) Data Processing: during the testing process, record the stress and displacement. If a peak shear stress is observed during the test with increasing shear displacement, it is taken as the shear strength. If no peak occurs, the shear stress at 4 mm displacement is adopted as the shear strength in accordance with the specimen size specifications of the Chinese geotechnical testing standard (GB/T 50123), with the test terminated at 6 mm displacement.
- For each condition, three parallel samples are tested, and the average strength is calculated. Based on the results, a shear strength—normal pressure plot is constructed to determine the cohesion and internal friction angle.







Figure 5: Sheared specimen.

2.4 Test Conditions

Naturally deposited snow requires compaction prior to utilization as an engineering material, with compacted densities typically surpassing 400 kg·m⁻³. Besides, interparticle friction within the snow impedes density beyond 700 kg·m⁻³ under mechanical compaction. Consequently, compacted snow specimens spanning densities of 450 to 650 kg·m⁻³ were selected in this study.

The effects of initial density ρ , sintering time t, and sintering temperature T_s were systematically examined through 69 test conditions, as detailed in Table 1.

Table 1 Test conditions.

Serial number	ρ (kg·m ⁻³)	t (days)	$T_{\rm s}$ (°C)	σ(kPa)
D-1	450,500,550,600,650	5	-5	25,50,75,100
D-2	450,500,550,600,650	5	-10	25,50,75,100
D-3	450,500,550,600,650	5	-20	25,50,75,100
t-1	450	0,1,3,5,10,15,20,30,60	-10	25,50,75,100
t-2	550	0,1,3,5,10,15,20,30,60	-10	25,50,75,100
t-3	650	0,1,3,5,10,15,20,30,60	-10	25,50,75,100
t-4	550	5,15,30	-5	25,50,75,100
t-5	550	5,15,30	-20	25,50,75,100
T-1	450	15	-5, -10, -15, -20, -25	25,50,75,100
T-2	550	15	-5, -10, -15, -20, -25	25,50,75,100
T-3	650	15	-5, -10, -15, -20, -25	25,50,75,100
T-4	550	1	-5, -10, -20	25,50,75,100
T-5	550	30	-5, -10, -20	25,50,75,100





3 Test Results and Analysis

3.1 Development Pattern of Shear Stress-Displacement Curves

Specimen deformation is characterized by shear displacement rather than strain in accordance with ISO 17892-10. Fig. 6 shows the shear stress-displacement curves at a shear rate of 0.8 mm·min⁻¹. The peak stress is defined as the shear strength when there is a peak in the curve; and the stress at a shear displacement of 4 mm is defined when there is no peak value.

During the initial shear stage, all curves rise steeply, indicating a rapid increase in shear stress with displacement. In the intermediate stage, the slope decreases, leading to a more gradual increase in stress. As shearing progresses, curves exhibiting a peak strength show a stress decline after a critical displacement; in contrast, those without a distinct peak either continue to rise at a minimal rate or stabilize.



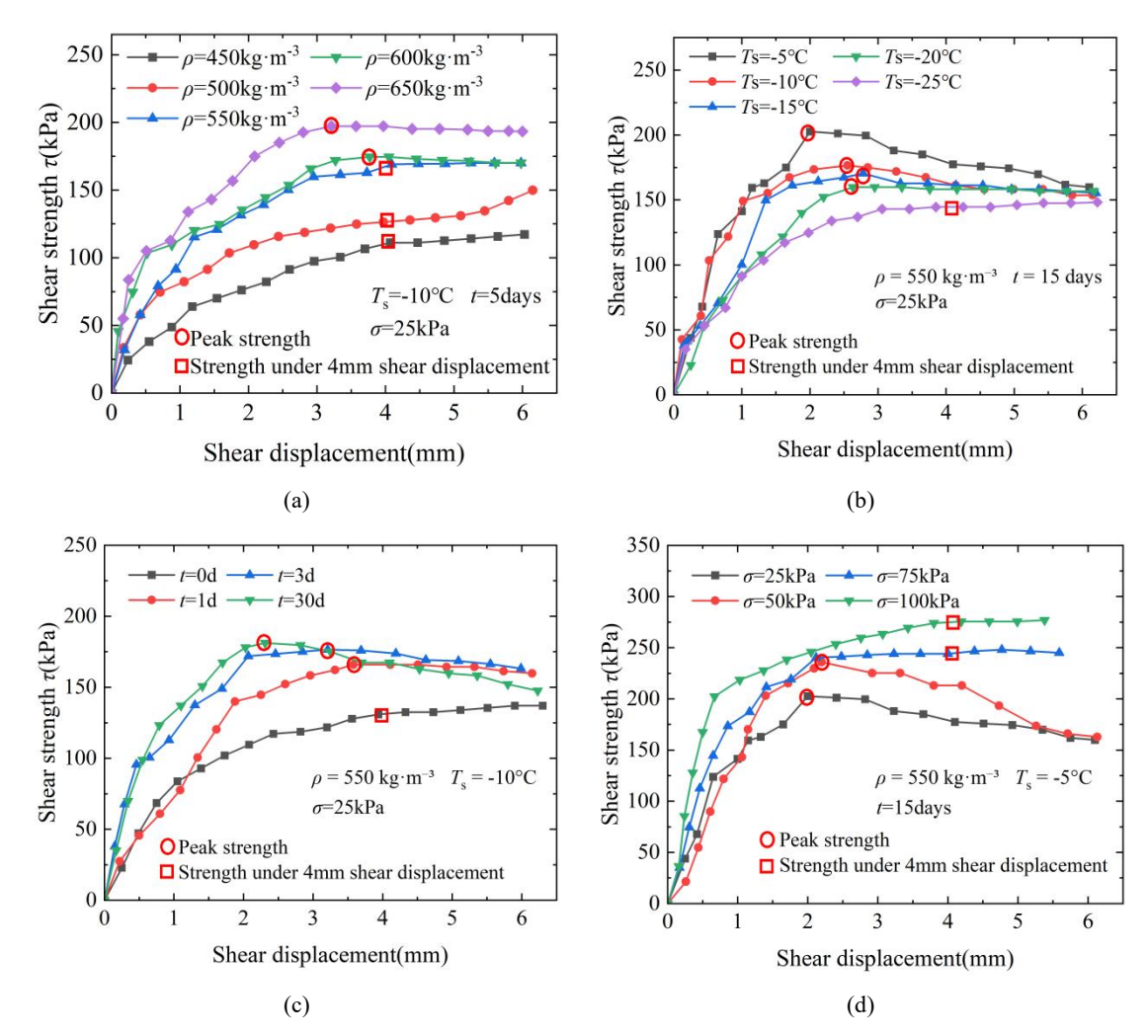






Figure 6: Shear stress-displacement curves under different test conditions ((a) Different densities; (b) Different sintering temperatures; (c) Different sintering times; (d)Different normal stresses).

155 Fig. 7 illustrates the development patterns of shear stress—displacement curves under other varying conditions: different densities (*T*_s = -10°C, *t* = 5 days), different sintering times (*ρ* = 650 kg·m⁻³, *T*_s = -10°C), and different sintering temperatures (*ρ* = 550 kg·m⁻³, *t* = 15 days), all tested under normal stresses ranging from 25 to 100 kPa. White indicates strain hardening (no peak strength), while dark shades represent strain softening (with peak strength). The color depth reflects the shear displacement at which peak stress occurs. The results show that strain softening is more likely to occur under conditions of high density, extended sintering time, elevated sintering temperature, and low normal pressure. In contrast, strain hardening tends to appear under opposite conditions. As discussed in Section 3.2, higher density, longer sintering duration, and higher sintering temperature are associated with increased sintering degree. Therefore, snow samples with greater sintering degree, when subjected to low normal pressure, tend to exhibit strain softening, and the higher the sintering degree, the smaller the shear displacement corresponding to the stress peak.

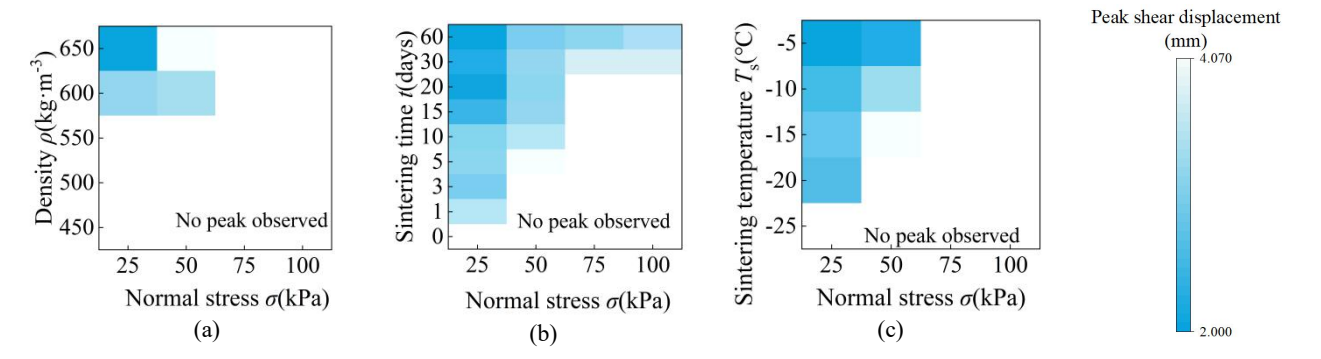


Figure 7: Development patterns of shear stress-displacement curves under varying influencing factors ((a) Different densities; (b) Different sintering times; (c) Different sintering temperatures).

3.2 Shear strength and shear strength parameters

170

175

Numerous studies (McClung, 1977; Barbero, 2016; Perla, 1977; Fyffe, 2007; Chiaia, 2008; Gaume, 2014) have adopted the Mohr-Coulomb criterion as the failure criterion for snow, which posits that shear strength increases linearly with normal stress, as expressed in Eq.(1):

$$\tau = c + \sigma \tan \varphi,$$
 (1)

where τ represents the shear strength, σ represents the normal stress, and c and φ represent cohesion and internal friction angle, respectively. The author conducted shear tests in advance within the normal stress range of 25 to 350 kPa. Fig. 8 presents the shear strength envelopes of compacted snow under different normal stresses, obtained from partial tests. It is evident that for snow samples with varying densities and in unsintered conditions, the shear strength increases linearly with





normal pressure up to 100 kPa. Beyond this threshold, the rate of increase in shear strength diminishes, indicating nonlinear behavior. In practical ice and snow engineering, the depth of snow foundations and the height of snow slopes are generally limited, resulting in relatively low overburden pressures. Therefore, normal pressures of 25, 50, 75, and 100 kPa were selected for calculating cohesion c and internal friction angle φ .

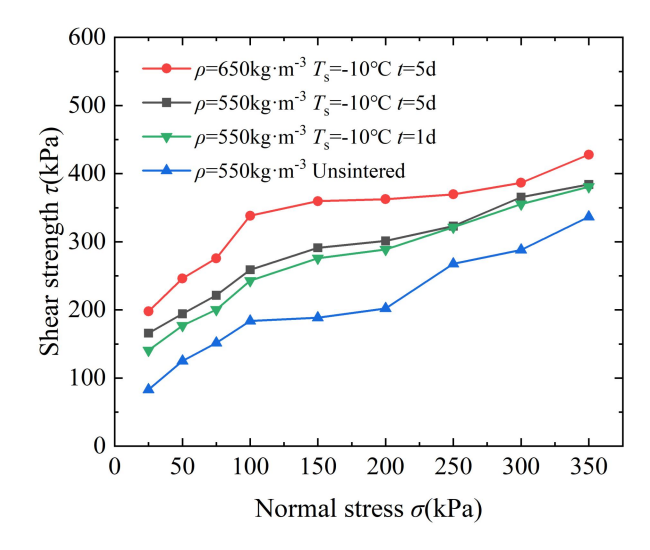


Figure 8: Shear strength envelope of compacted snow under varying normal stresses.

180 3.2.1 Effect of Initial Density

185

Fig. 9 presents the variation in shear strength of snow at initial densities ranging from 450 to 650 kg·m⁻³ after 5 days of sintering at -5 °C, -10 °C, and -20 °C. The results show that shear strength increases approximately linearly with density. For instance, at -10 °C, the shear strengths of snow samples with densities of 450 kg·m⁻³ and 650 kg·m⁻³ increased from 107.83 kPa, 136.06 kPa, 145.23 kPa, and 148.29 kPa to 197.86 kPa, 246.19 kPa, 265.70 kPa, and 338.22 kPa under normal stresses of 25, 50, 75, and 100 kPa, respectively.

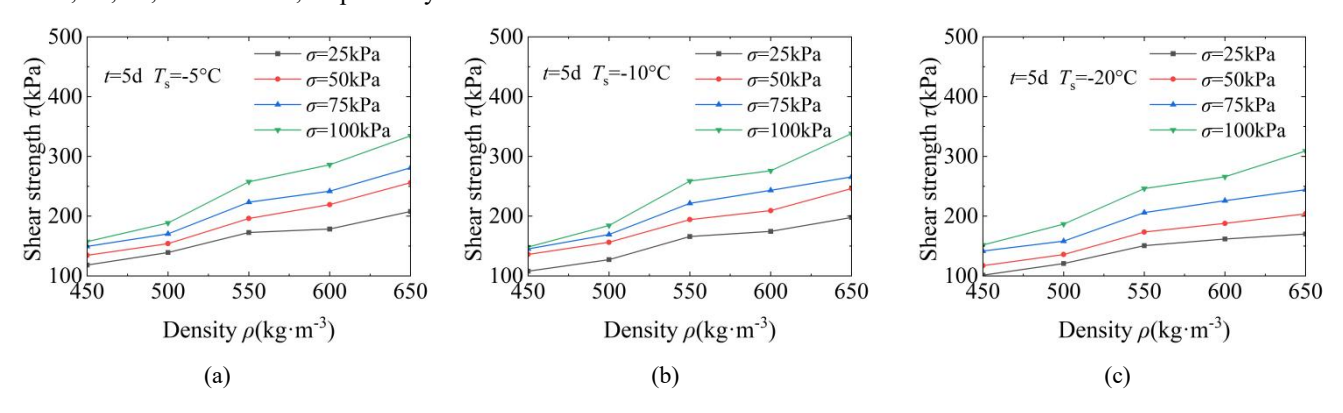


Figure 9: Variation of shear strength with initial density under different normal stresses after 5 days ((a) T_s =-5 °C; (b) T_s =-10 °C; (c) T_s =-20 °C).



190

195

200



Fig. 10 shows the corresponding changes in cohesion c and internal friction angle φ with varying initial densities under the same sintering conditions. Both parameters increase approximately linearly with density. As density increases from 450 kg·m⁻³ to 650 kg·m⁻³, cohesion rises from 106.83 kPa, 91.72 kPa, and 84.03 kPa to 168.60 kPa, 161.85 kPa, and 127.65 kPa at sintering temperatures of -5 °C, -10 °C, and -20 °C, respectively. Similarly, φ increases from 27.87 °, 32.71 °, and 35.10 ° to 58.29 °, 58.86 °, and 59.64 °, respectively. Notably, as density increases, the variation in internal friction angle across temperatures becomes smaller—at 650 kg·m⁻³, the difference is approximately 1°, whereas at 450 kg·m⁻³, it reaches up to 8 °.

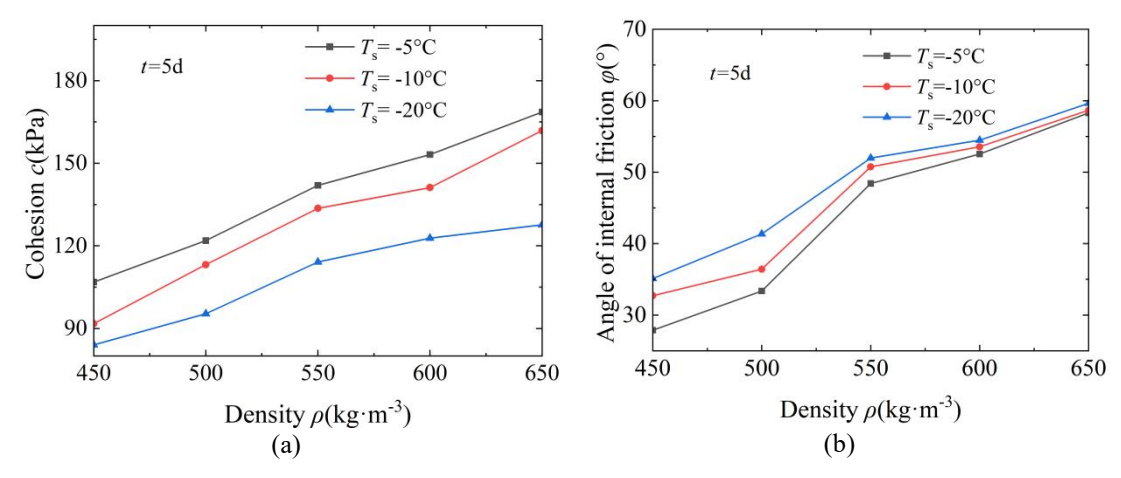


Figure 10: Variation of shear strength parameters at different initial densities after 5 days ((a) cohesion c; (b) Angle of internal friction φ).

3.2.2 Effect of Sintering Time

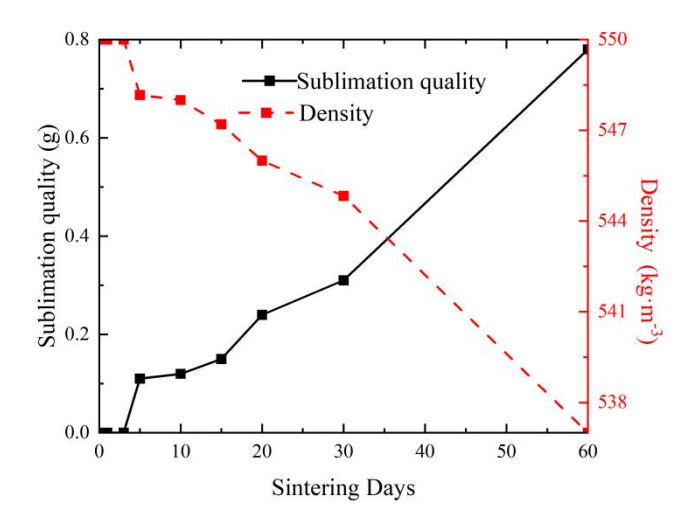
Fig. 11 shows the variation in sample density over different sintering times (using 550 kg·m⁻³ as a reference). It can be observed that density remains relatively stable during the first three days, followed by a gradual decline. By the 60th day of sintering, the sample mass decreased by 0.8 g, and the density decreased from 550 kg·m⁻³ to 537 kg·m⁻³. All specimens experienced identical absolute mass loss during same sintering days. This corresponded to a decrease in mass loss percentage from 2.96 % to 2.05 % as specimen density increased from 450 to 650 kg·m⁻³. This reduction is attributed to sublimation under sub-zero temperatures, where snow transitions directly from solid to gas, leading to a decrease in density.



210

215





205 Figure 11: Variation of average sublimation mass and specimen density with different sintering times.

Fig. 12 presents the variation in shear strength τ of snow samples with sintering time at initial densities of 450, 550, and 650 kg·m⁻³ under a constant sintering temperature of -10 °C. The shear strength exhibits a general trend of increase, stabilization, and subsequent decline with prolonged sintering time. This trend reflects the competing influences of sintering, which enhances strength, and sublimation, which weakens it. In the early stages of sintering, sintering dominates, leading to a significant increase in strength. In the middle to late stages, sublimation dominates, leading to a decrease in strength. The evolution of shear strength can be divided into three stages:

- (1) Rapid growth stage: in the early stages of sintering, bonding between snow grains develops quickly. Notably, the first day of sintering contributes significantly to the total strength, with negligible sublimation during this short period. As a result, the shear strength increases sharply.
- (2) Slowing growth stage: between 3 and 15 days, the strengthening effect of sintering diminishes, while the effects of sublimation become more apparent. Under the combined influence of sintering and sublimation, the shear strength fluctuates slightly but tends to stabilize. High-density samples $(650 \text{ kg} \cdot \text{m}^{-3})$ take 10-15 days to reach a steady strength, whereas lower-density samples $(450 \text{ kg} \cdot \text{m}^{-3})$ and $550 \text{ kg} \cdot \text{m}^{-3})$ stabilize only after 3 to 5 days.
- 220 (3) Strength decline stage: with extended sintering time, the sintering effect continues to weaken, and sublimation becomes the dominant factor, leading to a progressive reduction in shear strength.





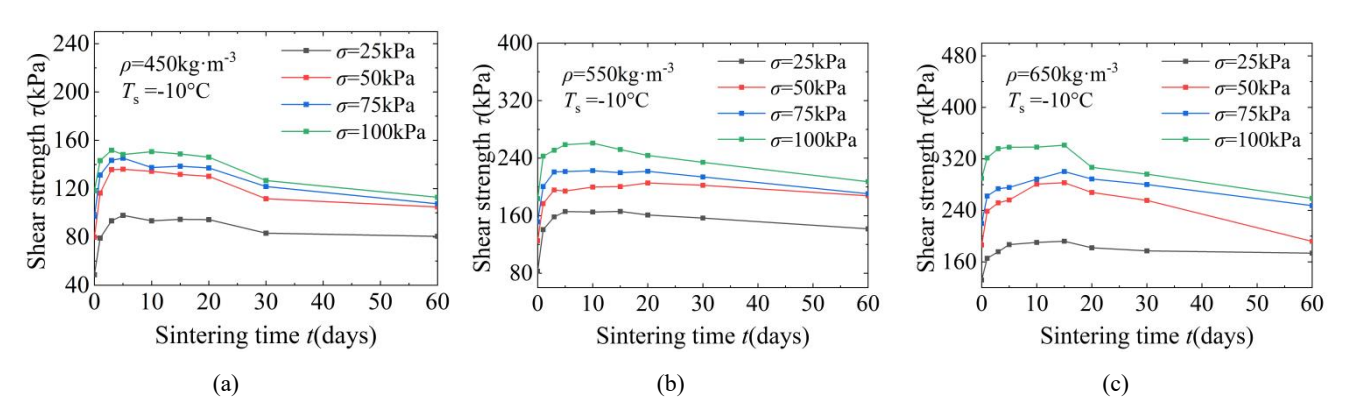


Figure 12: Variation of shear strength τ with different sintering times under sintering temperature of -10 °C ((a) ρ =450 kg·m⁻³; (b) ρ =550 kg·m⁻³; (c) ρ =650 kg·m⁻³).

Fig. 13 illustrates the changes in cohesion *c* and internal friction angle *φ* of snow samples with sintering time at the same three densities and sintering temperature. Cohesion *c* initially increases with time and then gradually declines, although it remains higher than that of unsintered snow even after 60 days. In contrast, the internal friction angle *φ* shows a marked decrease amounting to approximately 15 °, over time. This reduction may be attributed to the sintering-induced bonding between snow grains, which transforms the internal structure from loosely packed particles into a more continuous matrix, thereby reducing the interlocking frictional resistance.

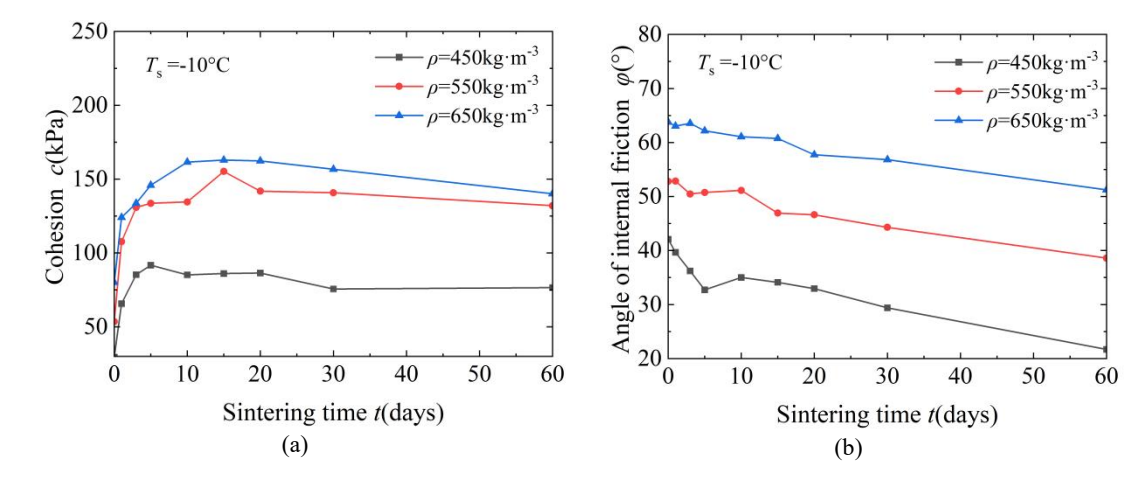


Figure 13: Variation of shear strength parameters with different sintering times under sintering temperature of -10 °C ((a) cohesion c; (b) Internal friction angle φ).

3.2.2 Effect of Sintering Temperature

Fig. 14 presents the variation in shear strength τ of snow samples with different sintering temperatures at densities of 450, 550 kg·m⁻³, and 650 kg·m⁻³ after 15 days of sintering. As sintering temperature increases, particle bonding accelerates,



245



significantly enhancing the shear strength of the samples. For example, at a density of 550 kg·m⁻³, the shear strengths at normal stresses of 25 kPa, 50 kPa, 75 kPa, and 100 kPa increased from 144.85 kPa, 178.41 kPa, 183.64 kPa, and 237.91 kPa at -25 °C to 202.64 kPa, 236.99 kPa, 243.52 kPa, and 274.82 kPa at -5 °C, respectively.

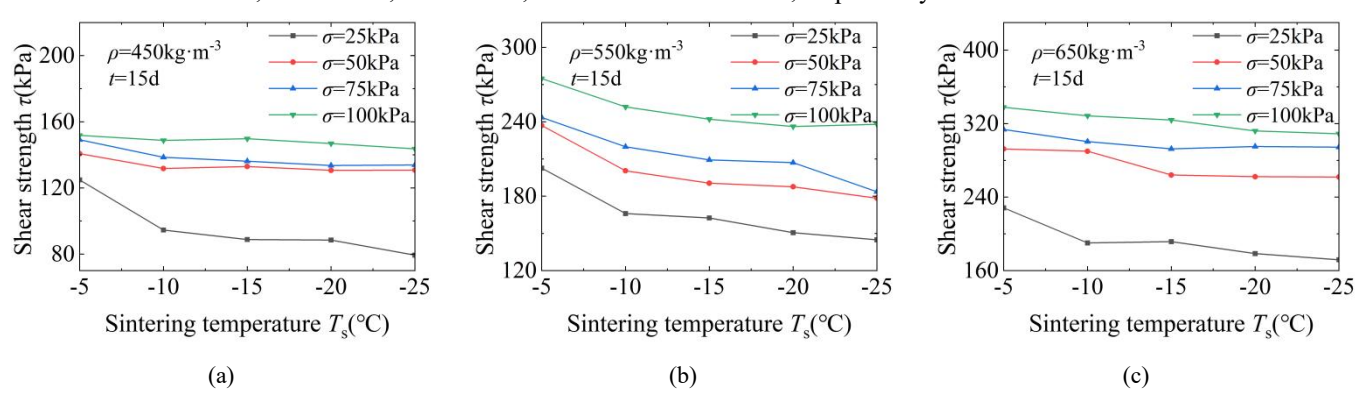


Figure 14: Variation of shear strength τ at different sintering temperatures after 15 days ((a) ρ =450 kg·m⁻³; (b) ρ =550 kg·m⁻³; (c) ρ =650 kg·m⁻³).

Fig. 15 shows the variation in cohesion c and internal friction angle φ of snow samples with different sintering temperatures under the same conditions. As the sintering temperature decreases, cohesion c declines by approximately 55 kPa, while the internal friction angle increases slightly. For samples with densities of 550 kg·m⁻³ and 650 kg·m⁻³, φ increases by about 6°, whereas for samples at 450 kg·m⁻³, the increase is more significant, reaching approximately 18°.

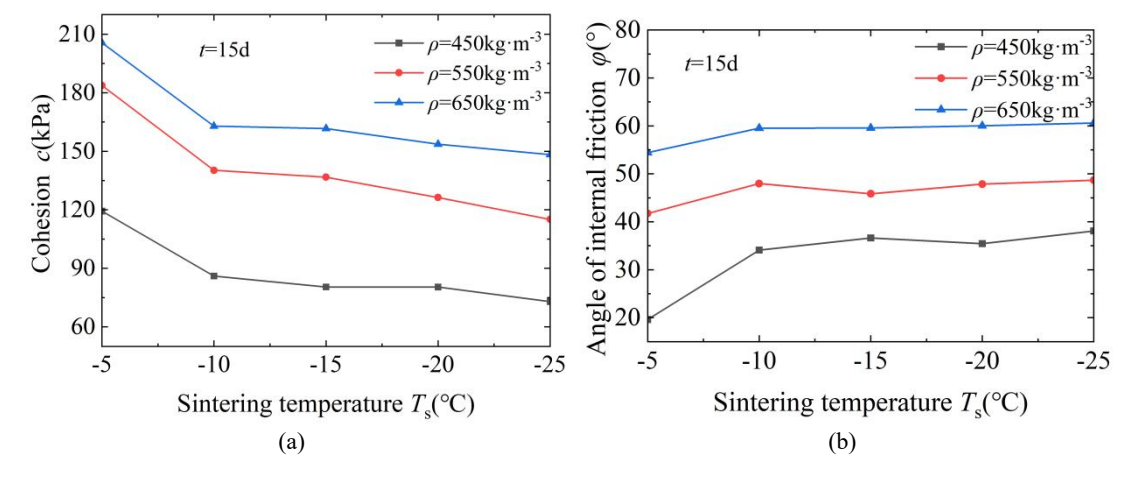


Figure 15: Shear strength at different sintering temperatures after 15 days ((a) cohesion c; (b) Internal friction angle φ).

4 Prediction Using GA-BP Neural Network

This section utilizes a genetic algorithm (GA) to optimize a back propagation (BP) neural network. Based on experimental data, a predictive model was developed with initial density, sintering time, sintering temperature, and normal stress as input





variables, and shear strength as the output variable. The model aims to explore the underlying relationships among these parameters.

4.1 Model Establishment

4.1.1 Data Collection and Preprocessing

A total of 276 experimental data points were collected, with 80 % randomly selected as the training set and the remaining 20 % used for testing. The data were scaled to the interval (0, 1) by applying max-min normalization, as defined in Eq.(2):

$$X_{norm} = \frac{X_i - X_{min}}{X_{max} - X_{min}},\tag{2}$$

where X_{norm} denotes the normalized value, X_i denotes the original input, and X_{max} and X_{min} denote the maximum and minimum values of the input variable, respectively.

260 4.1.2 BP Neural Network Model

The input layer of the neural network comprises four variables: density, sintering time, sintering temperature, and normal stress. The hidden layer consists of two sublayers, with 10 neurons in the first and 4 neurons in the second. The output layer contains one neuron representing the predicted shear strength. The architecture of the neural network is illustrated in Fig. 16.

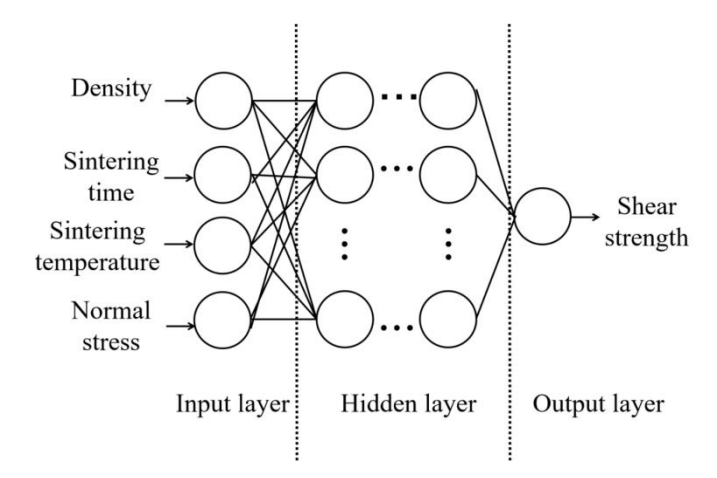


Figure 16: Neural network structure.

The ReLU (Rectified Linear Unit) function was selected as the activation function for the neural network, defined as Eq.(3):

$$265 f(x) = \max(0, x), (3)$$

The performance of the trained neural network model was assessed using the coefficient of determination (R^2), root mean square error (RMSE), and mean absolute error (MAE), which are defined as Eqs.(4) to (6):





$$R^{2} = 1 - \frac{\sum_{i=1}^{n} (y_{i} - \hat{y}_{i})^{2}}{\sum_{i=1}^{n} (y_{i} - \bar{y})^{2}},$$
(4)

$$RMSE = \sqrt{\frac{1}{n} \sum_{i=1}^{n} (y_i - \hat{y}_i)^2},$$
(5)

270
$$MAE = \frac{1}{n} \sum_{i=1}^{n} |y_i - \hat{y}_i|,$$
 (6)

where y_i denotes the actual value, \hat{y}_i denotes the predicted value, \bar{y} denotes the mean of the actual values, and n denotes the number of samples.

4.1.3 GA-BP Neural Network Model

To prevent the traditional *BP* algorithm from converging to local optima caused by randomly initialized weights, a *GA* was employed to optimize the *BP* neural network. The parameters used for the *GA-BP* neural network are summarized in Table 2.

Table 2 Parameters of the Genetic Algorithm.

Population Size	Crossover	Mutation	Number of	Encoding Length	
	Probability	Probability	Generations		
50	0.8	0.1	100	99	

The prediction workflow of the GA-BP neural network is shown in Fig. 17.





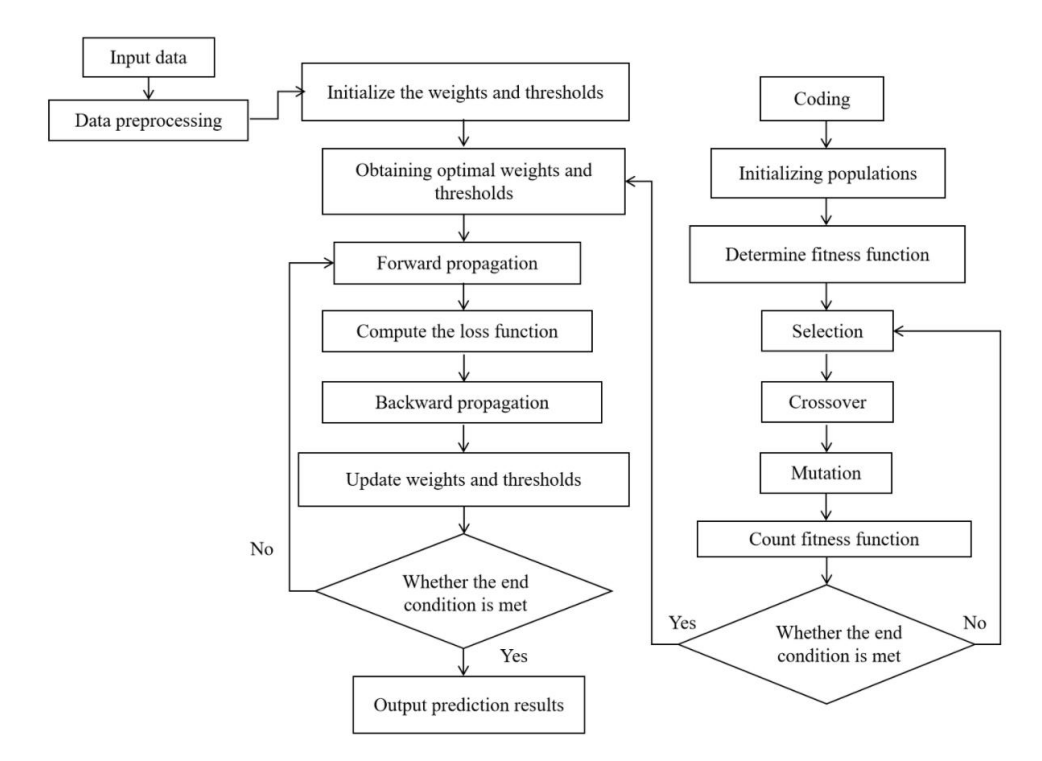


Figure 17: GA-BP neural network prediction process.

4.2 Prediction Results and Analysis

4.2.1 Model Parameter Analysis

280

285

290

The Spearman correlation coefficient matrix for shear strength τ , normal stress σ , sintering temperature T_s , sintering time t, and density ρ is presented in Fig. 18(a). The low correlation coefficients among normal stress, sintering temperature, sintering time, and density indicate that these variables are largely independent. The correlation coefficients between shear strength and normal stress, sintering time, sintering temperature, and density are 0.46, 0.27, 0.1067, and 0.76, respectively. The weak interdependence among input variables supports their appropriateness as model inputs. Among these, the variables most strongly correlated with shear strength, in descending order, are density, normal stress, sintering time, and sintering temperature. Fig. 18(b) illustrates the relative importance of each input variable to shear strength, calculated using the Connection Weights Method. Density exhibits the highest influence at 37.3 %, followed by sintering time and normal stress at 36 % and 20.3 %, respectively, while sintering temperature contributes the least at 6.5 %.





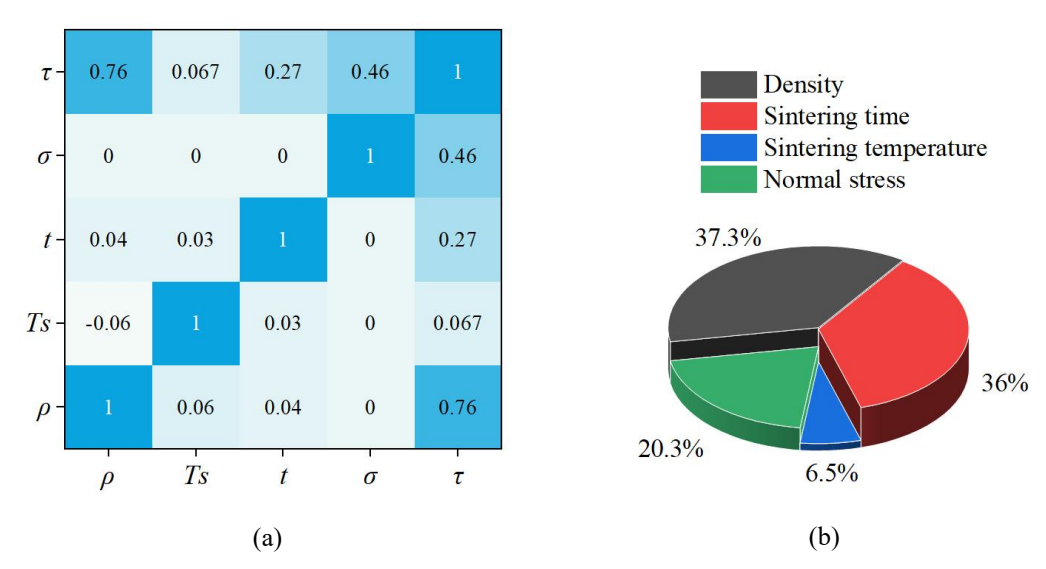
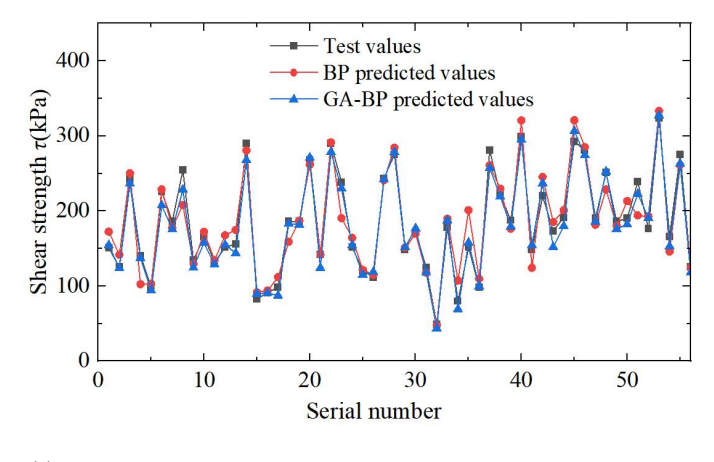


Figure 18: Analysis of model parameters ((a) Spearman's correlation coefficient matrix; (b) Relative importance of each parameter).

4.2.2 Neural Network Prediction Results

Fig. 19(a) compares the predicted and actual shear strength values for 56 test set data points using both the unoptimized *BP* neural network and the *GA-BP* neural network. Fig. 19(b) presents the relative errors of both models compared to the actual values. The relative errors of the *GA-BP* neural network remain below 15 % and are consistently lower than those of the unoptimized *BP* model, demonstrating that the *GA-BP* neural network offers superior predictive accuracy, greater precision, and improved applicability.



(a)



(b)

305

310



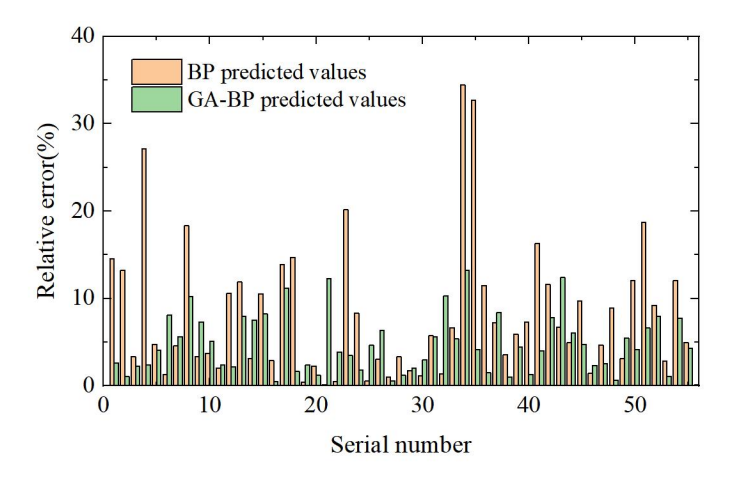


Figure 19: Prediction error of neural networks for shear strength estimation((a) Prediction value error;(b) Relative error of prediction value)

Fig. 20(a) and Fig. 20(b) illustrate the performance of the BP neural network and the GA-BP neural network on the training and test datasets. The GA-BP model demonstrates superior performance across all evaluation metrics— R^2 , RMSE, and MAE—compared to the traditional BP neural network. In the training set, the GA-BP model improved R^2 , RMSE, and MAE by 2.2 %, 40.81 %, and 37.90 %, respectively. For the test set, the corresponding improvements were 6.22 %, 45.04 %, and 39.74 %, as detailed in Table 3.

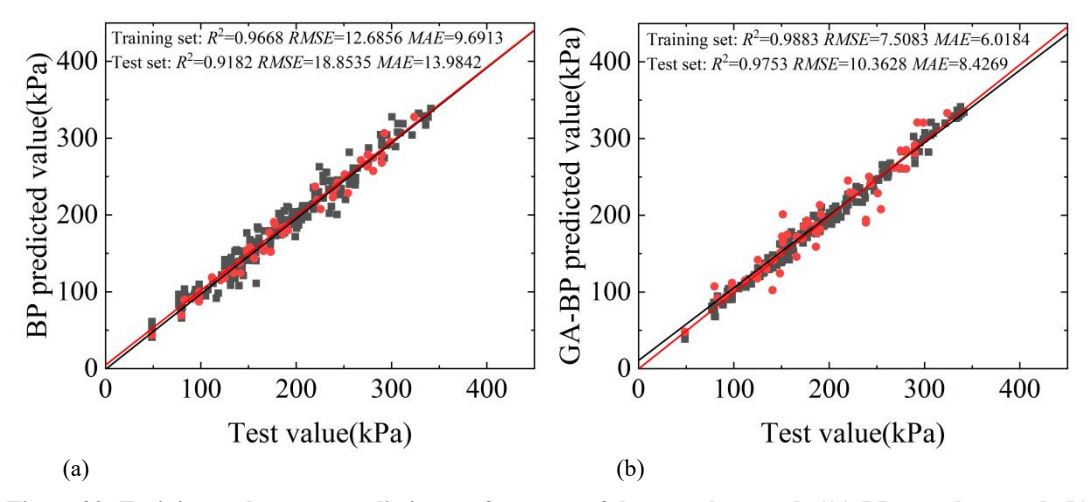


Figure 20: Training and test set prediction performance of the neural networks((a) BP neural network;(b) GA-BP neural network).

Table 3 Performance evaluation metrics for training and test sets.

R^2	RMSE	MAE



315



Training set (BP)	0.9668	12.6856	9.6913	
Training set (GA-BP)	0.9883	7.5083	6.0184	
Improvement ratio (%)	2.22	40.81	37.90	
Test set (BP)	0.9182	18.8535	13.9842	
Test set (GA-BP)	0.9753	10.3628	8.4269	
Improvement ratio (%)	6.22	45.04	39.74	

4.2.3 Prediction of Shear Strength Parameters

Based on the *GA-BP* neural network model, shear strength was predicted for various combinations of density (450 to 650 kg·m⁻³), sintering time (0 to 60 days), sintering temperature (-5 to -25 °C), and normal stresses of 25 kPa, 50 kPa, 75 kPa, and 100 kPa. These predicted values were used to derive the corresponding cohesion and internal friction angle, with the results summarized in Table 4.

Table 4 Neural network output results.

ρ	$T_{\rm s}$	t=1	d	t=:	5 d	t=10	0 d	t=1:	5 d	t=3	0 d	t=60) d
$(kg \cdot m^{-3})$	(°C)	c(kPa)	φ(°)	c(kPa)	φ(°)	c(kPa)	φ(°)	c(kPa)	φ(°)	c(kPa)	φ (°)	c(kPa)	φ(°)
	-5	83.21	27.74	106.79	21.57	110.16	22.07	116.40	21.90	97.74	20.52	80.57	19.05
	-10	80.19	27.91	90.94	30.70	95.99	28.61	98.27	26.70	81.82	25.54	64.43	25.34
450	-15	78.63	33.18	86.01	30.76	90.06	29.95	90.37	29.31	77.13	27.67	61.28	26.46
	-20	76.07	33.07	81.07	31.07	75.12	31.67	73.84	30.34	70.96	28.30	55.64	27.38
	-25	76.52	31.48	76.14	31.39	73.01	33.39	74.07	32.80	58.75	30.00	49.99	28.29
	-5	100.87	37.48	120.11	37.611	129.89	37.59	140.60	36.22	120.59	33.58	104.95	30.32
	-10	91.55	42.17	105.24	42.10	113.84	42.00	114.81	40.43	110.71	34.42	96.19	34.02
500	-15	93.24	42.28	96.98	44.13	103.21	43.77	109.54	40.70	99.11	36.37	91.44	34.24
	-20	91.26	42.18	94.54	42.57	100.58	42.24	104.39	41.19	93.85	36.04	86.21	34.16
	-25	89.27	42.09	87.11	44.62	92.05	43.81	97.91	40.51	92.59	33.96	81.57	34.49
	-5	112.22	51.65	135.02	50.54	141.02	50.66	170.88	43.59	155.83	40.91	124.34	34.87
	-10	107.97	52.15	125.70	52.33	125.04	51.73	135.70	47.68	131.94	44.64	122.65	38.52
550	-15	105.45	51.77	110.22	53.85	112.17	52.03	127.74	47.41	128.90	44.67	121.21	40.20
	-20	94.59	53.71	104.12	53.81	112.62	51.82	120.88	47.76	120.67	44.14	112.95	42.90
	-25	89.52	54.24	94.76	54.39	101.33	51.31	117.03	47.38	117.44	45.29	109.70	41.97
	-5	122.75	56.97	148.04	55.21	155.61	55.33	189.31	50.54	164.08	51.47	117.40	49.73
	-10	115.22	59.62	128.78	56.40	132.57	56.75	152.97	52.51	150.08	52.19	118.40	52.85
600	-15	107.81	59.45	121.14	57.46	124.01	57.55	145.22	53.06	153.75	52.88	117.89	52.13
	-20	104.41	57.99	112.60	56.73	115.44	56.73	127.92	55.80	133.39	53.63	114.89	53.13
	-25	95.51	57.62	97.34	57.42	102.44	57.88	126.49	55.56	126.55	55.00	114.30	54.51
650	-5	125.96	61.75	153.30	60.79	176.98	61.34	193.64	58.30	187.33	51.66	129.21	52.63



330



-10	124.69	62.14	139.15	61.96	155.15	61.84	151.50	62.55	167.01	54.70	128.69	54.44
-15	110.47	61.75	134.77	59.13	149.02	60.15	150.31	62.52	163.00	56.85	126.94	54.81
-20	100.80	61.25	129.98	59.36	141.57	60.01	150.94	59.58	163.98	56.83	120.94	56.33
-25	99.22	61.33	120.67	59.51	130.40	59.42	149.39	59.28	164.95	56.82	119.93	57.73

Fig. 21 presents the predicted cohesion *c* of snow samples with densities of 450, 550, and 650 kg·m⁻³ under varying sintering temperatures and sintering times. Cohesion *c* demonstrates a pronounced trend of initially increasing, then stabilizing, and eventually decreasing with extended sintering time across all densities. Furthermore, lower sintering temperatures consistently lead to reduced cohesion. The lowest cohesion values are observed in unsintered snow, while the highest are typically found at -5 °C and sintering times between 10 and 25 days. Notably, lower-density snow reaches its peak cohesion within a shorter sintering period.

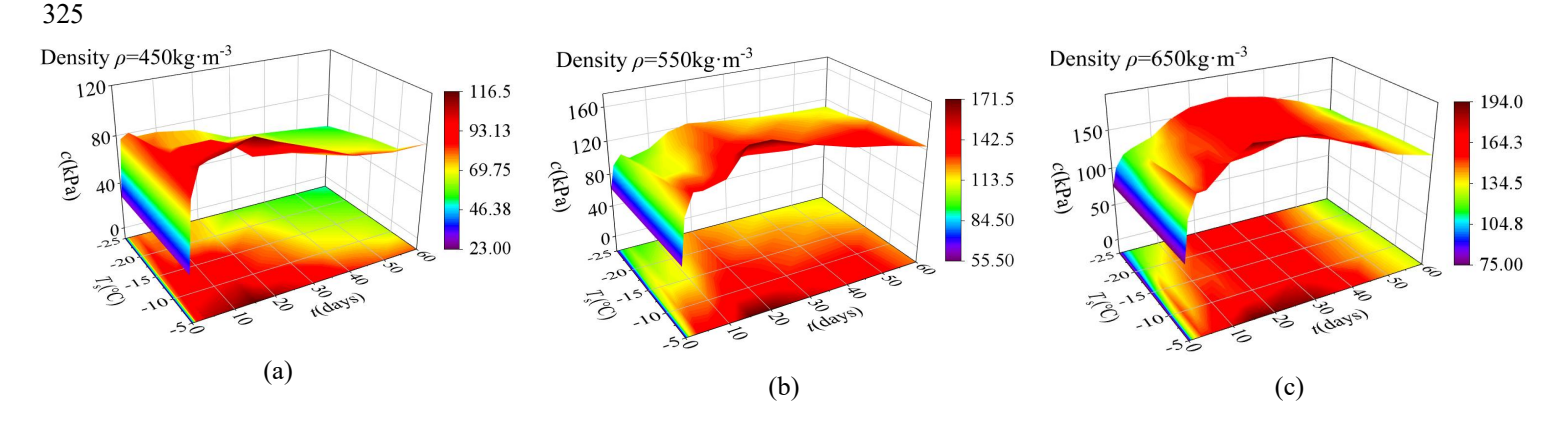


Figure 21: Predicted cohesion c values for various combinations ((a) ρ =450 kg·m⁻³; (b) ρ =550 kg·m⁻³; (c) ρ =650 kg·m⁻³).

Fig. 22 illustrates the predicted internal friction angle φ of snow samples with densities of 450 kg·m⁻³, 550 kg·m⁻³, and 650 kg·m⁻³ under various sintering temperatures and times. The internal friction angle consistently decreases with increasing sintering time, while it increases with decreasing sintering temperature. These trends align with the experimental results. At shorter sintering durations and lower sintering temperatures, snow exhibits higher internal friction angles. However, as sintering time progresses, φ declines, with the most pronounced reductions occurring at higher sintering temperatures (e.g., -5 °C).





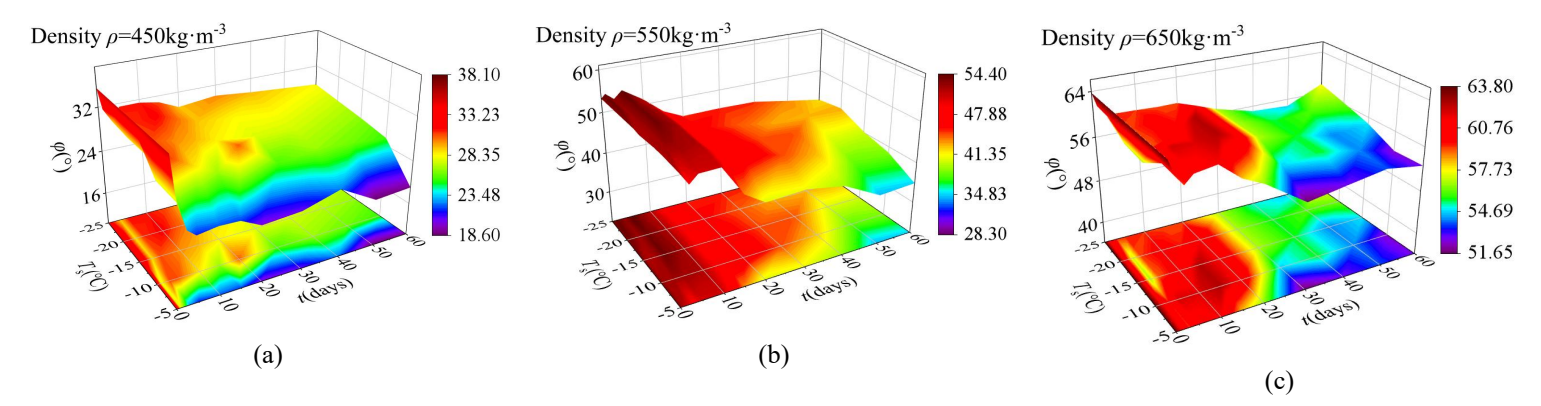


Figure 22: Predicted internal friction angle φ values for various combinations ((a) ρ =450 kg·m⁻³; (b) ρ =550 kg·m⁻³; (c) ρ =650 kg·m⁻³).

4.3 Discussion

335

350

355

Initial Density: Higher initial density indicates a greater number of snow particles per unit volume, leading to a more compact internal structure, stronger interparticle bonding, and more stable contact surfaces (Butkovich, 1958; Mellor, 1977). Consequently, both cohesion and internal friction angle increase with higher density.

Sintering Time: According to the water phase diagram shown in Fig. 23, under subzero temperatures, water reaches a dynamic equilibrium between its solid and gaseous phases via sublimation and condensation. In low vapor pressure environments, snow tends to sublimate into vapor, gradually reducing the density of compacted snow and weakening its strength. However, during sintering, clusters or bonding necks between particles continuously grow (Colbeck, 1979a, 1979b), enhancing mechanical strength. In the early stages of sintering, the strength enhancement due to cluster growth is dominant.
 In contrast, in later stages, sublimation effects prevail, leading to a strength decline. For individual snow particles, sintering causes surface morphology to become more regular (Bahaloo et al., 2024; Colbeck, 1983; Paterson, 1994; Wang, 1982; Zhuang, 2019), and the protrusions on contact surfaces tend to sublime first. This reduction in surface roughness may weaken the interlocking mechanism, resulting in a progressive decrease in internal friction angle during sintering.

It is noteworthy that the trend of decreasing strength for a certain sintering time has also been observed in previous findings (Jellinek, 1959; Zhuang, 2019; Fu, 2020), which reported similar results based on both field and laboratory studies. This trend is attributed to the interplay between sintering and sublimation processes. However, Abele (1990) reported through laboratory tests that the strength of compacted snow increases rapidly at first and then levels off without a subsequent decrease. This divergence may stem from differences in environmental water vapor pressure during sintering-sublimation is accelerated in dry environments, whereas it is suppressed in humid conditions. Therefore, in practical engineering applications, predictions of compacted snow strength evolution should take water vapor pressure into account.





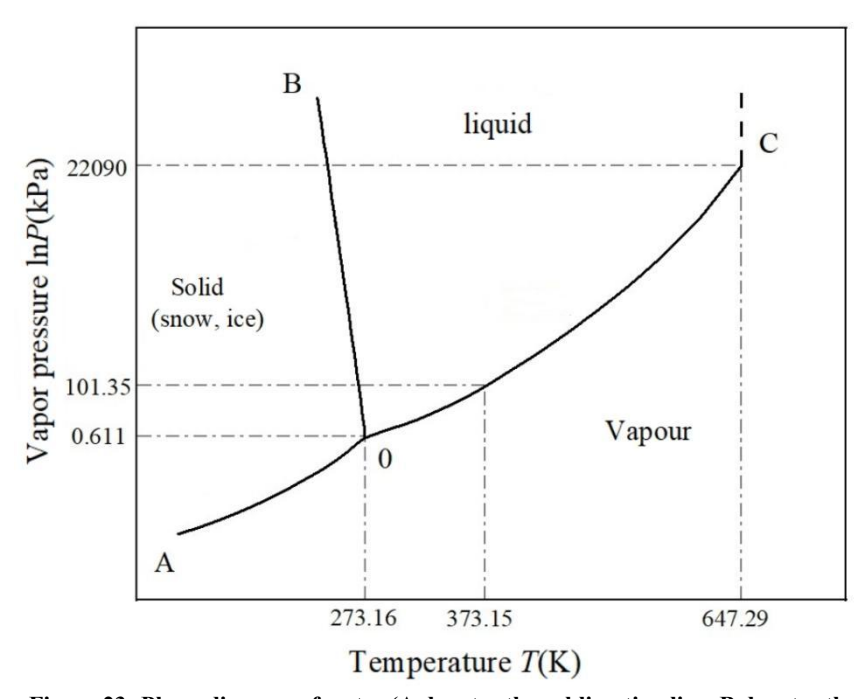


Figure 23: Phase diagram of water (A denotes the sublimation line, B denotes the melting line, and C denotes the evaporation line).

Sintering Temperature: As the sintering temperature increases, the mobility of water molecules is enhanced, accelerating cluster formation and resulting in more bonding structures between snow particles (Abele, 1967, 1990; Colbeck, 1983; Hong, 2022). During this process, snow grain transition from irregular to more regular shapes, which reduces surface roughness and subsequently leads to a decrease in the internal friction angle.

Shear rate: Numerous studies have demonstrated that shear rate significantly influences both strength and failure modes of snow. With increasing shear rates, shear strength first increases and then decreases, and transforming material behavior from strain hardening to softening (McClung, 1977; De Montmollin, 1982; Puzrin et al., 2019).

Other Factors: Beyond the variables discussed above, several other factors influence snow strength parameters significantly as well, including liquid water content, grain size and particle morphology. Snow with higher liquid water content tends to gain strength more rapidly at subzero temperatures, as the liquid water quickly freezes into ice. Experimental observations suggest that grain size strongly affects snow density—smaller grain are more easily compacted into dense snow. Grain morphology primarily impacts the internal friction angle; for example, hexagonal dendritic snow, with its irregular surface structure, may exhibit a higher internal friction angle compared to more uniformly shaped columnar snow.

5 Conclusions

360

365

370

Through laboratory direct shear tests and machine learning, the evolution patterns of shear stress-displacement curves, shear strength, and shear strength parameters of compacted snow were analyzed, leading to the following conclusions:

https://doi.org/10.5194/egusphere-2025-4768 Preprint. Discussion started: 20 October 2025

© Author(s) 2025. CC BY 4.0 License.



EGUsphere Preprint repository

375 (1) The shear stress-displacement curves of compacted snow exhibit two distinct development patterns: softening (with a

peak stress) and hardening (without a peak). Softening tends to occur under greater sintering degree conditions—such as

higher initial density, longer sintering time, and higher sintering temperature—and lower normal stress. Moreover, the

greater the degree of sintering, the smaller the shear displacement corresponding to the stress peak.

380 (2) As the initial density increases from 450 to 650 kg·m⁻³, both cohesion and internal friction angle show clear upward

trends. With increasing sintering time from 0 to 60 days, cohesion initially increases and then decreases, while the internal

friction angle consistently declines. As the sintering temperature decreases from -5 °C to -25 °C, cohesion continuously

drops, whereas the internal friction angle shows a corresponding increase.

385 (3) Neural network analysis revealed the relative influence of the main factors on shear strength: initial density (37.3 %),

sintering time (36 %), normal stress (20.3 %), and sintering temperature (6.5 %).

(4) Based on the GA-BP neural network, benchmark values of shear strength parameters were predicted for varying

combinations of three primary influencing factors.

This study focused on three key factors, which are initial density, sintering time, and sintering temperature. Other variables

such as water content, particle size, morphology and shear rate influence snow strength as well. When accounting for these

factors in engineering practice, adaptive adjustments should be implemented based on the benchmark framework established

in this study.

390

395

Code availability

The code used in this study is available upon request from the authors.

Data availability

400 Data will be made available on request.

Authorship contribution

Haifeng Huo: Conceptualization, Methodology, Formal analysis, Investigation, Data curation, Writing - original draft,

Visualization. Hui Xu: Conceptualization, Methodology, Resources, Supervision, Funding acquisition. Jixiu Wu: Validation,

405 Resources, Supervision. Tao Li: Validation, Resources, Supervision. Jingjin Liu: Validation, Resources, Supervision,

Funding acquisition. Enzhao Xiao: Validation, Supervision. Xueyuan Tang: Validation, Supervision.

Competing Interest





The contact author has declared that none of the authors has any competing interests.

Acknowledgments

The authors would like to express their gratitude for the financial support provided by the National Natural Science Foundation of China with Grant No.42576221.

415 References

410

- Abe, O.: Shear strength and angle of repose of snow layers including graupel, Ann. Glaciol., 38, 305 308, https://doi.org/10.3189/172756404781815149, 2004.
- Ager, B. H.: Snow road preparation in Scandinavia, Timber Canada, 2, 56-58, https://doi.org/10.4224/40001217, 1960.
- Abele, G.: Snow roads and runways, CRREL Monograph 90-2, US Army Cold Regions Research and Engineering Laboratory, Hanover, 1990.
- Abele, G. and Frankenstein, G. E.: Snow and ice properties as related to roads and runways in Antarctica, US Army CRREL Technical Report 190, Cold Regions Research and Engineering Laboratory, Hanover, ASIN B0007F4F4A, 1967.
- Barbero, M., Barpi, F., Borri-Brunetto, M., and Pallara, O.: An apparatus for in situ direct shear tests on snow, Exp. Tech., 40, 149–158, https://doi.org/10.1007/s40799-016-0019-7, 2016.
- Bahaloo, H., Forsberg, F., Lycksam, H., Casselgren, J., and Sjödahl, M.: Material mapping strategy to identify the density-dependent properties of dry natural snow, Appl. Phys. A, 130, https://doi.org/10.1007/s00339-024-07288-y, 2024.
 - Ballard, G. E. H., Feldt, E. D., and Toth, S. R.: Direct shear study on snow: procedures and data, CRREL Special Report 92, Cold Regions Research and Engineering Laboratory, Hanover, 1965.
- Barbero, M. et al.: An apparatus for in situ direct shear tests on snow, Test. Tech., 40, 149 158, https://doi.org/10.1007/s40799-016-0019-7, 2016.
 - Butkovich, T. R.: Strength studies of high-density snows, Eos Trans. AGU, 39, 305 312, https://doi.org/10.1029/TR039i002p00305, 1958.
 - Chiaia, B. M., Cornetti, P., and Frigo, B.: Triggering of dry snow slab avalanches: stress versus fracture mechanical approach, Cold Reg. Sci. Technol., 53, 170–178, https://doi.org/10.1016/j.coldregions.2007.08.003, 2008.
- 435 Colbeck, S. C.: Sintering and compaction of snow containing liquid water, Philos. Mag. A, 39, 13 32, https://doi.org/10.1080/01418617908239272, 1979a.
 - Colbeck, S. C.: Grain clusters in wet snow, J. Colloid Interface Sci., 72, 371 384, https://doi.org/10.1016/0021-9797(79)90340-0, 1979b.
- Colbeck, S. C.: Theory of metamorphism of dry snow, J. Geophys. Res. Oceans, 88, 5475 5482, https://doi.org/10.1029/JC088iC09p05475, 1983





- Colbeck, S. C.: Sintering in a dry snow cover, J. Appl. Phys., 54, 3327–3330, https://doi.org/10.1063/1.368684, 1983.
- De Biagi, V. et al.: Failure mechanics of snow layers through image analysis, Eur. J. Mech. A Solids, 74, 26 33, https://doi.org/10.1016/j.euromechsol.2018.10.018, 2019.
- De Montmollin, V.: Shear test on snow explained by fast metamorphism, J. Glaciol., 28, 187 198, https://doi.org/10.3189/S0022143000011898, 1982.
 - Demmenie, M., Woutersen, S., and Bonn, D.: Ice Sintering by Sublimation and Condensation, J. Phys. Chem. Lett., 16, 2104–2109, https://pubs.acs.org/doi/10.1021/acs.jpclett.5c00050, 2025.
 - Fohn, P. and Camponovo, C.: Improvements by measuring shear strength of weak layers, in: Proceedings of the International Snow Science Workshop, Banff, Canada, 1997, pp. 158–162.
- 450 Fu, X.: Test study on seasonal snow thermal properties and mechanical properties in Northeast China, M.S. Thesis, Northeast Agricultural University, https://doi.org/10.27010/d.cnki.gdbnu.2020.000222, 2020.
 - Fukuzawa, T. and Narita, H.: An experimental study on the mechanical behavior of a depth hoar under shear stress, in: Proceedings of the 1992 International Snow Science Workshop, edited by: Armstrong, R., Breckenridge, USA, ISSW, 171–175, 1993.
- Fyffe, B. and Zaiser, M.: Interplay of basal shear fracture and slab rupture in slab avalanche release, Cold Reg. Sci. Technol., 49, 26–38, https://doi.org/10.1016/j.coldregions.2006.09.011, 2007.
 - Gaume, J., Schweizer, J., van Herwijnen, A., Chambon, G., Reuter, B., Eckert, N., and Naaim, M.: Evaluation of slope stability with respect to snowpack spatial variability, J. Geophys. Res. Earth Surf., 119, 1783 1799, https://doi.org/10.1002/2014JF003193, 2014.
- Hong, J., Talalay, P., Man, T., Li, Y., Fan, X., Li, C., and Zhang, N.: Effect of high-pressure sintering on snow density evolution: Experiments and results, J. Glaciol., 68, 1107–1115, https://doi.org/10.1017/jog.2022.11, 2022.
 - International Organization for Standardization: Geotechnical investigation and testing Laboratory testing of soil, ISO 17892-10:2018, 2018.
- Jamieson, B. and Johnston, C. D.: Evaluation of the shear frame test for weak snowpack layers, Ann. Glaciol., 32, 59–69, https://doi.org/10.3189/172756401781819472, 2001.
 - Jellinek, H.: Compressive strength properties of snow, J. Glaciol., 3, 345–354, https://doi.org/10.3189/S0022143000017019, 1959.
 - Keeler, C. M. and Weeks, W. E.: Investigations into the mechanical properties of alpine snow-packs, J. Glaciol., 7, 253–271, https://doi.org/10.3189/S0022143000031038, 1968.
- Li, T., Huo, H., Hu, B., Jia, W. and Chen, Q.: Discrete element method analyses of the polar high-density sintered snow under the unconfined compression tests, Polar Res., 36, 240–253, https://doi.org/10.13679/j.jdyj.20220436, 2024.
 - McClung, D. M.: Direct simple shear tests on snow and their relation to slab avalanche formation, J. Glaciol., 19, 101–109, https://doi.org/10.3189/S0022143000215578, 1977.





- McClung, D. M.: Shear fracture precipitated by strain softening as a mechanism of dry slab avalanche release, J. Geophys.

 Res., 84, 3519–3526, https://doi.org/10.1029/JB084iB07p03519, 1977.
 - Mellor, M.: Engineering properties of snow, J. Glaciol., 19, 15–66, https://doi.org/10.3189/S002214300002921X, 1977.
 - Ministry of Housing and Urban-Rural Development of the People's Republic of China: Standard for geotechnical testing method, GB/T 50123-2019, China Planning Press, 2019.
- Nakamura, T., Abe, O., Hashimoto, R., and Ohta, T.: A dynamic method to measure the shear strength of snow, J. Glaciol., 56, 333–338, https://doi.org/10.3189/002214310791968502, 2010.
 - Paterson, W. S. B.: The physics of glaciers, 3rd edn., Pergamon Press, https://doi.org/10.1016/C2009-0-14802-X, 1994.
 - Perla, R.: Slab avalanche measurements, Can. Geotech. J., 14, 206–213, https://doi.org/10.1139/t77-021, 1977.
 - Perla, R., Beck, T. M. H., and Cheng, T. T.: The shear strength index of alpine snow, Cold Reg. Sci. Technol., 6, 11–20, https://doi.org/10.1016/0165-232X(82)90040-4, 1982.
- Podolskiy, E. A., Barbero, M., Barpi, F., Borri-Brunetto, M., Pallara, O., Frigo, B., Chiaia, B., Guillaume Chambon and Naaim, M.: Testing a new shear loading apparatus for in-situ studies of weak snow layers, in: ISSW 2013 Proceedings, https://hal.science/hal-00951689, 2013.
 - Podolskiy, E. A., Barbero, M., Barpi, F., Chambon, G., Borri-Brunetto, M., Pallara, O., Frigo, B., Chiaia, B., and Naaim, M.: Healing of snow surface-to-surface contacts by isothermal sintering, The Cryosphere, 8, 1651–1659, https://doi.org/10.5194/tc-8-1651-2014, 2014.
 - Putkisto, K.: Snow as a road-building material, National Research Council of Canada, Ottawa, https://doi.org/10.4224/20358958, 1959.
 - Puzrin, A. M., Faug, T., and Einav, I.: The mechanism of delayed release in earthquake-induced avalanches, P. Roy. Soc. A, 475, 20190092, https://doi.org/10.1098/rspa.2019.0092, 2019.
- Reiweger, I., Schweizer, J., Ernst, R., and Dual, J: Load-controlled test apparatus for snow, Cold Reg. Sci. Technol., 62, 119–125, https://doi.org/10.1016/j.coldregions.2010.04.002, 2010.
 - Schweizer, J.: Laboratory experiments on shear failure of snow, Ann. Glaciol., 26, 97 102, https://doi.org/10.3189/1998AoG26-1-97-102, 1998.
- Sun, B., Tang, X., Xiao, E., Shi, X., Cheng, X., Li, L., Wei, F. and Zhang, T.: Ice and snow runway engineering in the

 Antarctica: current status and prospect, Chin. J. Eng. Sci., 23, 161–168, https://doi.org/10.15302/J-SSCAE-2021.02.022,
 2021.
 - Wang, Y.: Metamorphosis of seasonal snow cover in the upper reaches of the Ili River in the Tianshan Mountains, J. Glacial Permafrost, 2, 63–72, https://doi.org/10.7522/j.issn.1000-0240.1982.0024, 1982.
- Wei, J., Lu, P., Hu, S., Zhao, Q., Yuan, S., Huo, P. and Wang, Q.: Research on the Evolution of Snow Crystal Necks and the Effect on Hardness during Snowpack Metamorphism, Water, 16, 48, https://doi.org/10.3390/w16010048, 2024.
 - White, G. and McCallum, A.: Review of ice and snow runway pavements, Int. J. Pavement Res. Technol., 11, 311–320, https://doi.org/10.1016/j.ijprt.2017.11.002, 2020.





- White, G., Outram, J., and McCallum, A.: Sintering of manufactured snow using liquid dye in a simulated environment, J. Cold Reg. Eng., 37, 04023007, https://doi.org/10.1061/JCRGEI.CRENG-694, 2023.
- Yamano, K. and Endo, Y.: Dependence of shear strength of snow cover on density and water content, J. Jpn. Soc. Snow Ice, 64, 443–451, https://doi.org/10.5331/seppyo.64.443, 2002.
 - Zhuang, F.: Experimental Study on Snow Hardness and Its Testing Technology, M.S. Thesis, Dalian University of Technology, https://doi.org/10.26991/d.cnki.gdllu.2019.000727, 2019.